Energy considerations in spraying process of a spill-return pressure-swirl atomizer

JEDELSKÝ, J.; JÍCHA, M.

Applied Energy
2014, vol. 132, November 2014, pp. 485-495

ISSN: 0306-2619

DOI: https://doi.org/10.1016/j.apenergy.2014.07.042

Accepted manuscript

Energy considerations in spraying process of a spill-return pressure-swirl atomizer

Jan Jedelsky* and Miroslav Jicha

Faculty of Mechanical Engineering, Brno University of Technology, Technicka 2896/2, 616 69 Brno, Czech Republic

Abstract

The work focuses on energy conversion during the internal flow, discharge and formation of the spray from a pressure-swirl (PS) atomizer in the simplex as well as spill-return mode. Individual energy forms are described in general and assessed experimentally for a particular PS atomizer and light heating oil as a medium. The PS spray was observed at various loads to investigate the liquid breakup process and the spray characteristics. Spatially resolved diameters and droplet velocities, measured by means of phase-Doppler anemometry, served for estimation of the energy characteristics in the PS spray.

The input energy given by the potential energy of the supplied liquid partially converts into the kinetic energy (KE) in the swirling ports with hydraulic loss in per cent scale. Most of the pressure drop is associated with rotational motion in the swirl chamber with total conversion efficiency at the exit orifice ~58%. The rest of the input energy ends up as friction loss, leaving room for improvement.

The overall value (ID_{32}) of the Sauter mean diameter of droplets in the spray, D_{32}, varies with pressure drop Δp_l powered to –0.1. The radial profiles of D_{32} widen with the increase in spill/feed ratio (SFR), but the ID_{32} remain almost constant within the studied SFR range. The spray KE at closed spill line covers the droplet KE (21–26%) and that of entrained air (10–13%), both moderately varying with Δp_l. The specific KEs of both the liquid and air markedly drop down with the spill line opening.

Atomization efficiency is less than 0.3% for the studied range of operation regimes and depends on Δp_l and SFR. Our results confirm low power demand of simplex PS atomizers, with extra energy consumption in spill mode. Several recommendations are given for PS atomizer innovations and development of new, more efficient, designs meeting more stringent environmental requirements.

Keywords

Pressure-swirl atomizer, Spill-return, Atomization efficiency, Energy conversion, Sauter mean diameter, Spray formation

1. Introduction

Atomization of liquids is a process during which bulk liquid is transformed into fragments or small droplets; the process is accompanied with a significant increase in the interfacial area and consumes the energy introduced to the liquid at the atomizer inlet. The nature of the feed energy[1] determines the atomization process. Thus, from the energy point of view, an atomizer can be considered a device that converts the input energy, E_i, into the increased surface tension energy of sprayed liquid, E_A. Effectiveness of the conversion is characterised by the atomization efficiency: $\eta_a = E_A/E_i$. Its knowledge allows comparison of different types of atomizers and improvement of the spray quality. The quality of the atomization process is frequently described using the Sauter mean diameter (SMD or D_{32}) [1] of the final droplets in the spray; the smaller the SMD the better the spray is. It is crucial namely in combustion applications; the SMD of a sprayed fuel strongly affects the combustion process, namely the stability limits, combustion efficiency and pollutant emission levels. Good atomization quality promotes the fuel evaporation and decreases the demand of ignition energy [2]. A properly designed atomizer is thus a prerequisite for efficient combustion and optimal use of energy resources through proper utilization of the chemical energy contained in expensive fossil liquid fuels.

Bayvel and Orzechowski [3] show all traditional atomizers work with very small η_a, typically below 0.1%, and that any spray quality improvement requires disproportionally more energy as η_a drops down. For example, a pressure atomizer generating 100 µm droplets has η_a = 0.05–0.07% and to reduce the diameter to 50 µm causes the efficiency to drop to the order of several thousandths per cent. Rivette and Evers [4] calculated atomization

* Corresponding author. Tel.: +420 541 143 266; fax: +420 541 143 365.
E-mail address: jedelsky@fme.vutbr.cz (J. Jedelsky).

[1] It is either the potential energy of the liquid in pressure atomization, the electric energy for ultrasonic and electrostatic atomizers, or the mechanical power for rotary atomizers etc.

efficiencies of compound pressure nozzles ranging from 0.4 to 1% according to the injection pressure. They observed that increasing the velocity of the fluid is an increasingly inefficient method of creating the turbulence necessary for drop formation. Dumouchel *et al.* [5] also studied compound nozzles and found their atomization efficiency in range 0.9–2.6% depending on their design rather than on injection pressure. Loefler-Mang and Leuckel [6] investigated the atomization process of spill controlled pressure-swirl (PS) atomizers and found remaining surface energy of droplets between 0.1 and 0.4% of the initial static pressure energy. Petela [7] applied an exergetic approach to the pressure and airblast atomization. He found the exergetic efficiency of the pressure atomization for inlet pressures in the order of 0.1–1 MPa is below 1% and it decreased with the growth in the inlet pressure. Sovani *et al*. [8] compared the performance of a conventional pressure injector with an effervescent Diesel injector (DI) designed for fuel injection into Diesel engines. They found the pumping energy required for delivering fuel with their effervescent DI operating at an injection pressure of 18 MPa and 2% gas to liquid ratio (GLR) is over five times smaller than that required by a conventional DI operating at 150 MPa for comparable D_{32} value. We [9] studied the energy conversion in an effervescent atomizer for inlet pressures of 0.1–0.5 MPa with 2–10% GLR and shown its η_a is less than that of PS atomizer for the same spray quality. Lefebvre [10] evaluated the efficiency of airblast atomizers and found it to be 0.007. Several spraying methods, developed for specific purposes, work more efficiently than PS atomization; the roller atomization with η_a = 30% and ultrasonic atomization with energy requirement less than 100 J/kg of atomized particles [11].

PS atomizers are widely used in industrial and domestic burners, utility boilers [12], gas turbine combustors [13], in aviation engines [14], direct injection gasoline engines [15], rocket engines [13], and many other engineering areas thanks to their simple design, low energy demands and good atomization characteristics required for high quality combustion with minimum emissions. A drawback of the simplex PS nozzles is the poor atomization quality at low flow rates, where inlet pressures are reduced. This disadvantage has been overcome by the spill-return PS nozzles. Above cited works give important information on the atomization characteristics of simplex PS atomizers and other spraying techniques as well but spill-return PS atomizers are only sporadically referred to. A detailed description with an analysis of the entire energy conversion process of simplex and namely spill-return PS atomizers is, to the best of our knowledge, absent in the literature. In this paper, we address some aspects of the energy conversion process during PS atomization. An experimental study of PS atomizer was performed in simplex as well as spill-return mode with the aim to estimate the individual energy ratios during the internal flow, discharge and formation of the spray. An analysis of the energy processes reveals possibilities for innovative designs of PS atomizer with increased spraying efficiency.

2. Experimental facility

The experimental data included in this work were acquired during cold testing of a PS atomizer in the Spray laboratory at the Brno University of Technology. Following paragraphs describe essential experimental equipment used including the atomizer under test, cold test bench with the fluid supply system and PDA system.

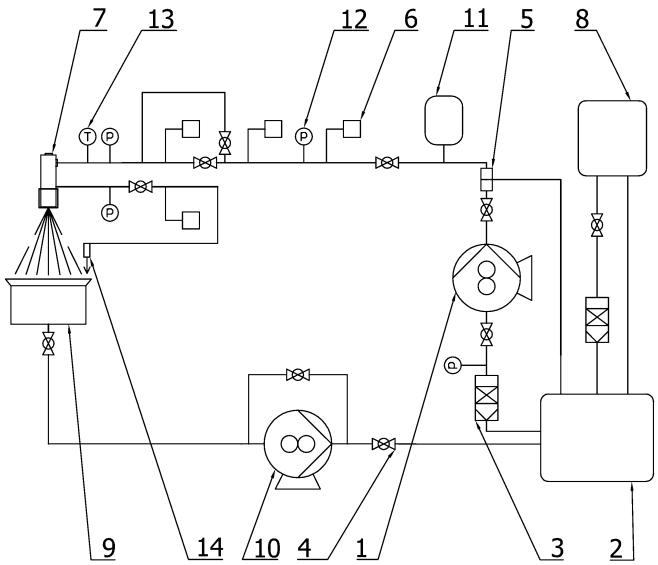

Fig. 1. Schematic layout of the experimental facility.

2.1. Cold test bench

A schematic layout of the test bench is shown in Fig. 1. It consists of a gear feed pump (1) that supplies fuel from a main tank (2) through filters (3), control valves (4, 5) and flow meters (6) into the atomizer (7). A chiller (8) controls the fuel temperature hence its viscosity. The spray falls into a collector (9) and then it is returned to the main supply tank by a pump (10). The collector is connected to a fuel mist separator that keeps the spray zone free of aerosol but does not substantially disturb the spray. The fuel piping is equipped with a hydraulic shock absorber (11) placed in front of the atomizer. Flow rate of spill-return atomizers at given inlet pressure Δp_l is controlled by a regulating valve at its spill return line (14). The feeding and return lines are equipped with flow meters, pressure (12) and temperature (13) readings. Uncertainty in fluid pressure measurements is 16 kPa. Uncertainty of the fluid temperature measurements is 0.4 °C. Uncertainty of the volumetric flow rate measurements is 5% of the measured value. Uncertainty values of the different instruments are taken from the manufacturer's supplied datasheets.

2.2. Atomizer description and operation

A spill-return PS atomizer, working originally in a high-power stationary oil burner, was used for this study. The nozzle (Fig. 2) is placed in a body which provides an inlet, distribution and return of fuel and gripping to a 3D computer controlled support. Fuel is fed into a swirl chamber through four tangential ports of a square cross-section. The swirl chamber contains a cylindrical entry part followed by a conical part and exit orifice of small length-to-diameter ratio. The spill return line is placed in the nozzle axis at the top cap and opens using a regulating valve.

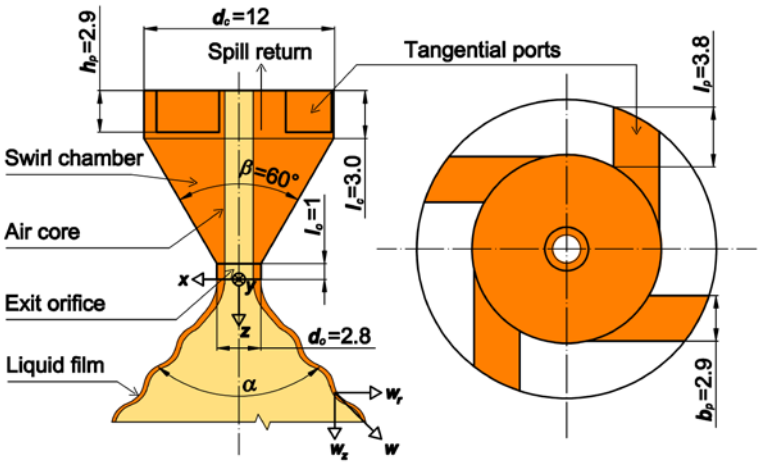

Fig. 2. Schematic layout of the atomizer with main dimensions in millimetres. The coordinate system is identical with that in Fig. 3.

The atomizer was continuously operated with a vertical downward position of the main axis. All tests were done with one batch of light heating oil (LHO) which simulates real hydrocarbon fuel. LHO is suitable testing fluid as it is not as volatile as other primary fuels [16]. It was chosen as the Newtonian model fluid also as its atomization-important properties (viscosity, surface tension and density) are close to these of other fuels sprayed with PS atomizers frequently, such as diesel fuel [8, 17], No. 2 heating oil, kerosene [2, 18, 19], petrol [20-22], non-renewable fossil fuel substitutes (e.g. biodiesel, E10 [23, 24]), crude or residual oil [13] and waste fuels. Physical properties of the LHO at room temperature are: σ = 0.0297 kg/s^2, ρ_l = 874 kg/m^3, μ_l = 0.0185 kg/(m·s), c_l = 2400 J/(kg·K). The viscosity was measured using an Ubbelohde viscometer (uncertainty value 7%). We used the detach method to measure the surface tension (uncertainty value 5%), the density was specified in a certified laboratory and the c_l value was taken from literature. The temperature of LHO was kept during all tests at 20 ± 1 °C to ensure constant physical properties of the liquid. Operational conditions of spill-return atomizer are described by two independent factors: the pressure differential between the nozzle inlet and exit, Δp_l, and the spill/feed ratio[2] (SFR or ε).

2.3. Phase-Doppler analyzer

Time-resolved size and velocity of droplets were measured using a commercial phase-Doppler analyzer (PDA) by Dantec Dynamics. This 1-component classical PDA system is equipped with a standard optics; basic parameters are given in Table 1, and its configuration with the coordinate system is shown in Fig. 3.

[2] reciprocal value of the excess liquid coefficient

Measurements of the spray using PDA were made as radial scans with equidistant sampling in radial positions r_j = 0, 5, 10, ..., 90 mm, at axial distance from exit orifice z = 100 mm with $n = 2^{13} = 8192$ particles measured at each point j. We found this number of droplets statistically sufficient for estimation of D_{32} in PS sprays; note that other experimenters [25] acquired only 3,000 validated samples while in [26] acquiring 20,000 drops was stated to ensure sufficient statistical reliability of optical measurement results in PS sprays. Three scans in angular positions shifted by 30° were always performed and resulting $D_{32,j}$ at radial position r_j was obtained by averaging the values of the three measurements at a given r_j. This averaging was necessary as the PS sprays are not perfectly axially symmetrical and also for statistical reasons.

Table 1
Configuration of PDA system.

Parameter	Value
Laser	Ar–Ion$^+$ 300mW
Wavelength	514.5 nm (up to 90 mW)
Beam waste diameter	0.82 mm
Transmitting optics	Dantec 58N10
Beam separation	60 mm
Bragg frequency	40 MHz
Front focal length of transmitting and receiving optics	500 mm
Receiving optics	Dantec 57X10, three photo-detectors
Scattering angle φ	67.6°
Elevation angle	0.68°
Polarization	Parallel (horizontal)
Scattering mode	First-order refraction
Signal processor	Dantec 58N50

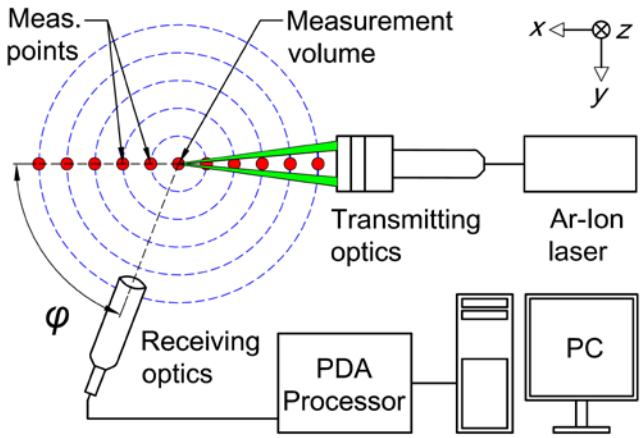

Fig. 3. Set-up for the PDA measurements.

3. Results and discussion

Operation of PS atomizer is analysed in a consecutive manner with an emphasis on the energy transfer during the atomization process. The first part deals with internal flow, discharge and sheet formation for a range of atomizer loads. Liquid breakup and spray macrostructure are elucidated with the use of spray photography. PDA is used to provide spatially resolved distributions of droplet characteristics such as diameters and velocities. Efficiency of the spray production is calculated and compared with other atomization techniques.

3.1. Internal flow, discharge and sheet formation

The operating principle of PS atomizers relies on the conversion of liquid pressure into kinetic energy (KE) to achieve high relative velocity between the liquid emerging from a nozzle and the surrounding gas. The input energy in non-reacting pressure atomization is predominantly driven by the potential energy of the supplied liquid at a

pressure drop Δp_l between the atomizer inlet and exit; all other inlet energy forms can be neglected[3]. The process is considered isothermal with no preheat or cooling. Thermal effects such as vaporization of the atomized liquid (LHO is a non-volatile liquid) or exchange of heat between the discharged liquid and the surrounding air are thus unimportant. A part of the inlet energy is lost during the energy conversion due to friction and dissipation of turbulence; it turns into heat, which amount linearly increases with the inlet pressure. The rise in the liquid temperature between the atomizer inlet and exit $\Delta T = (1-\eta_n)\Delta p_l/(\rho_l c_l)$, assuming the adiabatic conditions and constant nozzle efficiency $\eta_n = 0.56$, is ~0.4 °C for $\Delta p_l = 2$ MPa only. Our measurement of ΔT (the difference between supply line temperature and temperature in near nozzle spray) using paired thermometers for $\Delta p_l = 0$–2 MPa shown a linear tendency between Δp_l and ΔT (with correlation coefficient $R^2 = 0.99$ for the linear fit). The predicted ΔT values were in whole Δp_l range systematically by ~20% higher than the measured ones. This difference can be explained with heat transfer between the liquid and the nozzle surface inside and heat transfer between the liquid and surrounding air outside the atomizer. The linearity between Δp_l and ΔT suggests for constant η_n value, which is analysed bellow and confirmed using other methods.

3.1.1. Internal flow

Part of the inlet pressure energy converts into KE in the supply channel and swirling ports; the value is ~1% of the inlet energy independently of the operation pressure. Oil flow in these ports has a laminar character with Reynolds number $\mathrm{Re_p} = 316$–898 for the observed range of $\Delta p_l = 0.2$–2 MPa. Specific hydraulic loss in rectangular swirling ports, predicted according the Darcy–Weisbach equation with Darcy friction factor $f_D = 64/\mathrm{Re_p}$ in duct systems, is:

$$e_{hp} = \frac{\Delta p_p}{\Delta p_l} \cong 8\mu_l \sqrt{\frac{n_p}{k_{p1} A_p}}\, k_{p2} \left(1 + k_{p1}\right)^2 \frac{w_p}{\Delta p_l} \qquad (1)$$

where $k_{p1} = b_p/h_p$, $k_{p2} = l_p/b_p$ and $A_{pT} = n_p h_p b_p$. Eq. (1) has a minimum for $k_{p1} = 1/3$, so swirl ports with $b_p = 0.\overline{3} h_p$ are to be used to reduce the loss. The e_{hp} is relatively low — in unit per cent scale for our nozzle. The flow velocity and cross-sectional area affect the flow downstream and spray formation, and cannot be simply changed to minimize the loss. Tipler and Wilson [27] recommend the length to width ratio of ports, k_{p2}, should not be less than 1.3, as short slots discharge the liquid in a diffused manner and may result in an uneven spray. Short ports also do not steer the flow tangentially enough. So the port length should be set to the recommended value of 1.3 b_h but not larger to keep the pressure loss low. The minimum sufficient number of the swirl ports, n_p, providing homogeneous swirling flow and a uniform spray [28] should be used, as large port number also negatively affects the loss.

The oil enters a swirl chamber in the tangential direction producing strongly vortical flow with an air core in the nozzle centerline. This flow is relatively complex [29] with a dominant swirling velocity component containing vortices of various types [30-33]. Significant part of the remaining pressure drop converts into KE at the exit orifice and partly dissipates due to viscous effects in the liquid and by friction on the inner walls while the surface energy rise due to the establishment of the air core is minor. Hydraulic loss in the cylindrical part of the swirl chamber can be, assuming simple helical flow, very roughly rated as:

$$\Delta p_c \propto 0.5 \rho_l^{a+1} \mu_l^{-a} d_c^{\,a-1} l_c w^{a+2} \qquad (2)$$

where a depends on the character of the flow and for our case, where $\mathrm{Re_W} = 2830$–8940 according Walzel [34], $a \cong 0.3$. The chamber loss increases with the chamber length, l_c, and decreases with its diameter, d_c. Changing d_c complexly affects the spray quality as well as spray cone angle (SCA or α), so its simple enlargement to reduce the Δp_c is not applicable. The chamber length should be kept short to minimize frictional loss, however, sufficient length must be provided for the separate jets issuing from the swirl ports to coalesce into a uniform vortex sheet [35]. Other work [36] suggests that higher values of the length/diameter ratio of swirl chamber, l_c/d_c, up to a maximum of 2.75 result in improved atomization.

The total energy loss inside the atomizer is characterised by the nozzle efficiency η_n and the velocity coefficient c_w[4], where $\eta_n = c_w^2 = \rho_l w_o^2 / 2\Delta p_l$ is the efficiency of the input energy conversion into KE at the nozzle exit. Using our PDA data for the near nozzle velocity of the liquid phase and approximating the velocity decay curve to the exit orifice, we found $\eta_n = 0.59$ for $\Delta p_l = 1$ MPa; η_n moderately decreases with Δp_l (see Table 2). Note that other authors [6, 37] report even lower values as $\eta_n = 0.1$–0.4 while Horvay and Leuckel [38, 39] measured $\eta_n = 0.42$–0.66

[3] KE of the liquid delivered to the atomizer is ~0.2% of the inlet pressure energy for inlet pipe diameter of 10 mm, independent of Δp_l. Original surface energy and potential energy term due to gravity (for a height of 0.2 m) are less than 0.006% and 0.9% respectively at $\Delta p_l = 0.2$ MPa, and both of them are inversely proportional to Δp_l. Fluid compressibility contributes negligibly to total energy input for the pressure drops in MPa scale.

[4] It compares real discharge velocity with the theoretical one for an ideal nozzle working with inviscid liquid.

depending on the shape of the convergent part of the swirl chamber and Yule with Chinn [40] found for large PS atomizers η_n = 0.73–0.86. The key role of the swirl chamber is to provide a thin liquid film with high-speed injection into still ambient air. The requirement of the highest available velocity (and so the maximised velocity coefficient) is in apparent contradiction with the requirement for the thinnest possible liquid film (which is conditioned by complex internal flow). It explains the wide range of nozzle efficiencies reported by different authors. The internal energy loss, given as $1 - \eta_n$, is typically 42%. Just a few per cent of this loss belongs to the swirl ports; most of the energy is spent in the swirl chamber so any optimization efforts should target to improvement of the chamber flow.

3.1.2. Discharge and sheet formation

The photographic documentation of the PS spray was made to observe the breakup process and to acquire overall information on the spray macrostructure, see Figs. 4 and 5. The liquid flows through the discharge orifice in an annular form and spreads as a conically shaped film, due to conversion of the tangential velocity component into the radial one, increasing its surface and interacting with the ambient air. The exit velocity is proportional to the square root of Δp_l. The initial film thickness at the exit orifice:

$$t_o = \frac{\dot{Q}_{lo}}{\pi d_o}\sqrt{\frac{\rho_l}{2\Delta p_l \eta_n}} \tag{3}$$

The film envelope widens with the axial distance z from the nozzle exit which causes its thinning into a membrane like form. Assuming simple attenuation of the film, with no surface waving, perforations and agglomeration, its thickness downstream the nozzle is

$$t(z) = \frac{t_o d_o}{d_o + 2z \cdot tg\,\alpha/2} \tag{4}$$

The film thickness, at the exit orifice, moderately varies with flow conditions as $t_o \propto \mathrm{Re}_W^{-0.1}$ (in good agreement with [41, 42]), and it is ~0.5 mm thick (this value correspond to results in [30, 43] after scaling according to the nozzle size) for Δp_l = 0.2 MPa, which corresponds to the surface energy e_{Ao} equal to 0.01% of the inlet energy. The e_{Ao} decreases with Δp_l. This slightly wrapped and waved thin layer of liquid faces a propagation of instabilities within the liquid as well as over the liquid surface, caused by the high slip velocity between the liquid film and the ambient gas.

Table 2
Atomizer characteristics with spill return line closed.

Δp_l (MPa)	$\dot{Q}_{lo}$ (ml/s)	η_n (%)	L[a] (mm)	SCA[a] (°)	t_L[b] (mm)	ID_{32} (μm)	e_{AL} (%)	η_a (%)	e_{kD}[c] (%)	e_{kg}[d] (%)
0.2	77.5	–	82	–	–	–	–	–	–	–
0.4	106	–	57	41	0.04	–	0.40	–	–	–
0.6	128	–	29	43	0.07	–	0.15	–	–	–
0.8	145	–	15	43	0.11	–	0.07	–	–	–
1.0	160	58.9	10	44	0.14	87.2	0.04	0.20	25.8	9.7
1.2	174	56.8	12	44	0.12	85.7	0.04	0.17	22.9	9.4
1.4	187	58.0	10	44	0.13	84.1	0.03	0.15	22.8	10.4
1.6	199	55.7	10	44	0.14	83.6	0.03	0.13	21.2	11.2
1.8	210	52.9	10	45	0.13	82.6	0.02	0.12	21.4	12.3
2.0	221	55.9	11	45	0.13	81.4	0.02	0.11	21.1	13.5

[a] Based on photographic documentation.
[b] Calculated according Eq. (4).
[c] Calculated according Eq. (6) using PDA data.
[d] Calculated according Eq. (7) using PDA data.

The magnitude of the surface irregularities grows up with the distance from the nozzle until it causes ruptures and consequent breakup of the liquid membrane. Only surface wave instabilities were found to initiate the sheet breakup, contrary to [44], where two sheet atomization regimes (perforations and surface waves) were documented. The mean breakup length[5] was measured using spray photography and is documented in Table 2 together with the relative surface energy at the breakup position, e_{AL}. At low Δp_l, ~0.2 MPa, the liquid film shows an onion stage; the surface tension forces dominate and overcome the radial momentum which causes the film to collapse. The film does

[5] It is the average length of the liquid sheet measured on the sheet envelope from the exit orifice to the point where the sheet is no continuous any more.

not break up until the collapse point and atomizes poorly afterwards (Fig. 4) with dripping character of the breakup process[6]. The spray shape changes with increasing Δp_l to a tulip-like one with still inferior atomization. Primary atomization of the entire liquid volume completes at $\Delta p_l > 0.4$ MPa in a large distance from the nozzle exit. With further increase of Δp_l, the atomization improves, and the breakup point approaches the exit orifice due to the increased relative gas-to-liquid velocity. Also, the SCA slightly widens (see Table 2). At common operating pressures, units of MPa, the discharged mass takes a form of fully developed hollow cone spray. Further change of Δp_l does not significantly affects the SCA any more; its value is practically given by the internal nozzle geometry; this effect was also seen by Mandal *et al.* [45]. This variable effect of Δp_l, on SCA can be approximated as $SCA \propto \Delta p_l^{0.05}$ in reasonable agreement with [37] who for similar nozzle and Δp_l, report $SCA \propto \Delta p_l^{0.11}$. Ballester and Dopazo [12] for smaller PS atomizer found $SCA \propto \Delta p_l^{0.42}$. Such different trends suggest for sensitivity of the momentum transfer during discharge to internal flow conditions.

Table 3
Atomizer characteristics with varying spill/feed ratio at Δp_l = 2 MPa.

ε	$\dot{Q}_{lo}$ (ml/s)	η_n (%)	L[a] (mm)	SCA[a] (°)	t_L[b] (mm)	ID_{32} (μm)	e_{AL} (%)	η_a (%)	e_{kD}[c] (%)	e_{kg}[d] (%)
0	221	55.9	11	45	0.13	81.4	0.024	0.11	21.1	13.5
0.43	164	34.1	11	50	0.11	83.6	0.026	0.06	6.5	3.5
0.58	140	18.6	10	54	0.13	84.6	0.023	0.04	3.1	1.4
0.69	119	9.9	12	59	0.13	84.7	0.024	0.03	1.2	0.8

[a, b, c, d] The same meaning as in Table 2.

Opening of the spill valve (Fig. 5) causes a part of the liquid to divert from the swirl chamber to the spill return line. The swirl momentum of the liquid inside the nozzle retains but the flow rate through the exit orifice reduces so the ratio between the axial and the radial velocity downstream the nozzle drops down causing the spray cone to expand markedly as documented in Table 3 and Fig. 5. The observed spray structure and its variation with Δp_l are in accordance with the findings described in [2, 12, 46].

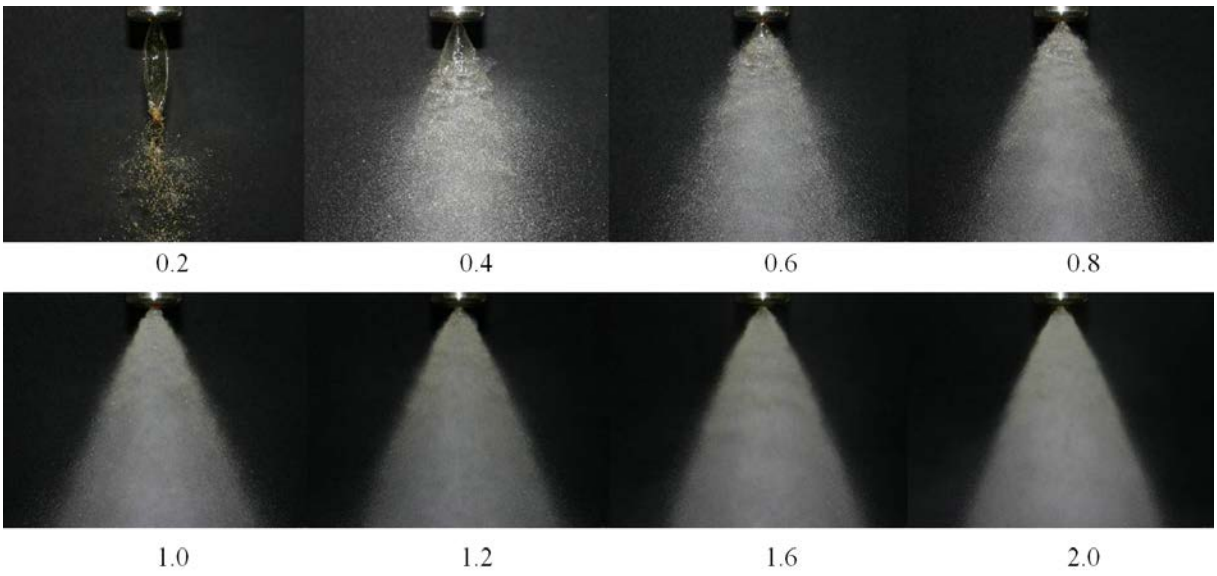

Fig. 4. Spray structure at varying Δp_l (MPa), spill return line closed.

[6] This poor atomization quality at low loads is retrieved with spill return control.

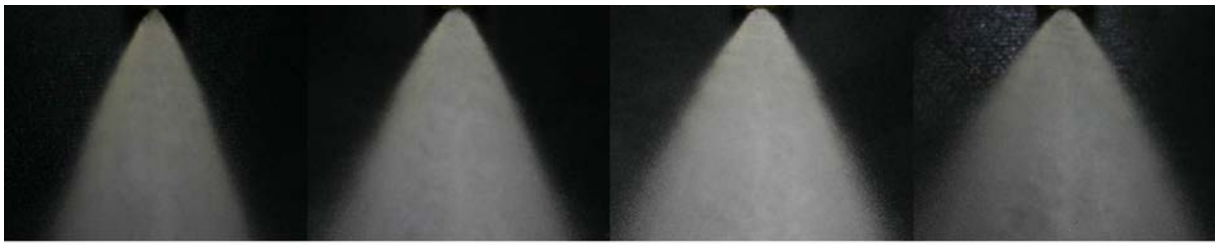

Fig. 5. Spray structure at Δp_l = 2 MPa, SFR varied.

3.2. Liquid breakup and spray characteristics

The instabilities in the liquid sheet increase with distance and cause its breakup into ligaments, filaments and finally into drops in the form of a hollow cone spray. Further disintegration of drops into smaller droplets occurs further downstream from the nozzle orifice and is driven by the collision between droplets and the action of aerodynamic forces [3].

The mean droplet size in developed spray varies significantly with the radial position, as illustrated in Fig. 6. The D_{32} is ~40 µm in the centreline and increases up to almost 120 µm on the spray border at Δp_l = 1 MPa. Drop size larger at the spray edge results from the droplet and gas dynamics in the spray cone and was also found by Yule *et al.* [40] and others. Increase in Δp_l leads to a reduction of the size at radial distances r > 15 mm. The opposite trend near the centreline can be explained by enhanced mixing at greater pressures and transfer of larger droplets into the area. However, the spray in r < 20 mm is of low importance as it contains less than 3% of the total liquid mass in all inspected regimes. Small droplets with D_{32} < 60 µm fill the central part of the spray cone as they are dislocated there from the main stream by the air movement. 80% of liquid mass is placed within r = 30–50 mm and large (heavy) droplets are formed in the outer part of the spray.

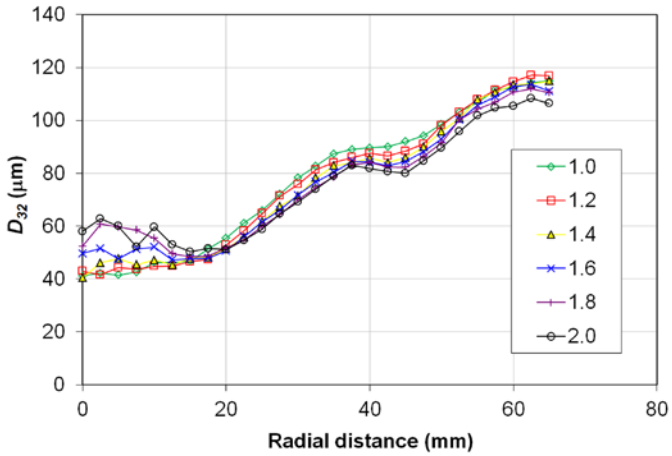

Fig. 6. Radial distribution of D_{32} at varying Δp_l (MPa), z = 100 mm, return line closed.

To characterise this wide size range of droplets in the radial profile with a unique parameter we introduce an integral Sauter mean diameter, ID_{32}, calculated according Eq. (A.2) of the Appendix. Table 2 shows that ID_{32} monotonically decreases with Δp_l as expected and in accordance with published data. The trend can be approximated by:

$$ID_{32} \propto \Delta p_l^{-b} \tag{5}$$

where b = 0.10 with correlation coefficient R^2 = 0.99. By doubling the inlet pressure, ID_{32} drops by 7%. Other authors [13, 47, 48] who investigated the relation between D_{32} and Δp_l, refer b = 0.23–0.33 (reported here after a correction for the effect of the pressure on the flow rate, as flow rate is considered an independent factor in these works) for similar PS atomizers and operation conditions. This large difference can be partly explained by different measurement methods used, as described in the Appendix and proposed in [49] or by experimental conditions. Also, rheological properties of the atomized liquid play an important role (described in Section 3.4 and [50]). Other reason can be the range of radial positions where they measured the D_{32}. For example, our data give $D_{32} \propto \Delta p_l^{-0.17}$ at the position of the maximum liquid flux (r = 42.5 mm). Different trends would be found for other droplet statistics such

as arithmetic mean diameter, D_{10}, or mass mean diameter, $D_{v0.5}$, due to the difference in size distributions. Note that the ID_{32} at z = 100 mm, where the breakup is completed (see explanation in Section 3.3), is in a constant ratio to the sheet thickness, estimated according Eq. (4) at the characteristic breakup position, for the whole range of the Δp_l as shown in Table 2: $t_L \cong 1.6 ID_{32}$. We, therefore, deduce that the variation of droplet size with Δp_l change depends on the effect of Δp_l on the relative liquid-to-air velocity rather than on the effect of Δp_l on the sheet formation. Using our formula $ID_{32} \propto \Delta p_l^{-0.1}$, we estimate that an improvement in nozzle efficiency by 10 percentage points, due to eventual chamber redesign, would reduce the ID_{32} by 1.6%. A chamber modification producing a sheet with reduced thickness could have a stronger impact.

The D_{32} profiles for the cases of the return line opening (Fig. 7) seem to drop down with the increase in SFR but these curves rather shift to greater radial positions with the spray widening (documented by the spray photography in Fig. 5 above) as it is also suggested by the almost constant ID_{32} values in Table 3 within the studied SFR range. The negligible effect of SFR on the ID_{32} is in agreement with [51].

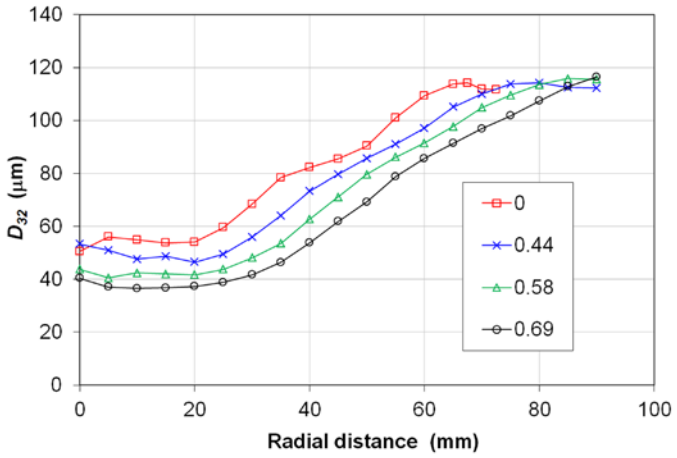

Fig. 7. Radial distribution of D_{32} at Δp_l = 2 MPa, SFR varied, z = 100 mm.

3.3. Kinetic energy of droplets and air

The KE of the spray contains the energy of moving droplets and the energy of the entrained mass of ambient air. These energies can be estimated separately using the PDA data. The specific KE of liquid (droplets):

$$e_{kD} = \frac{E_{kD}}{E_i} = (1-\varepsilon)\frac{\rho_l}{2\Delta p_l}\sum_{j=1}^{m} r_j \sum_{i=1}^{n_j} D_{ij}^3 w_{Dij}^2 \Big/ \sum_{j=1}^{m} r_j \sum_{i=1}^{n_j} D_{ij}^3 \qquad (6)$$

where D_{ij} is the diameter of an individual droplet i at the radial distance from the atomizer axis r_j. Its velocity, w_{Dij}, was estimated by $w_{Dij} = w_{zDij}\sqrt{z^2 + r_j^2}/z$ with the tangential velocity component neglected (it is typically one order of magnitude lower than axial component w_{zDij}). An axially symmetrical spray and equidistant sampling distance $\Delta r_j = r_j - r_{j-1}$ were assumed.

Specific KE of the surrounding air entrained by the sprayed liquid:

$$e_{kg} = (1-\varepsilon)\frac{\pi\rho_g}{\Delta p_l \dot{Q}_l}\sum_{j=1}^{m} \Delta r_j r_j w_{gj}^3 \qquad (7)$$

where the mean air velocity at position j is calculated as $w_{gj} = \frac{1}{n_j}\sum_{i=1}^{n_j} w_{zDij}$, using the individual velocity of droplets, w_{zDij}, as an estimate of the local air velocity; only droplets with low Stokes number, typically < 0.2, which are assumed to follow the flow field well, are included. The smallest, often satellite, droplets were not taken into account.

Individual velocities estimated using PDA in position 100 mm downstream the exit orifice at Δp_l = 1 MPa and spill return line closed are shown in Fig. 8. The difference between mean velocity of liquid mass $w_{lj} = \left(\sum_{i=1}^{n_j} D_{ij}^3 w_{Dij}^2 \Big/ \sum_{i=1}^{n_j} D_{ij}^3\right)^{1/2}$ and mean velocity of entrained air, $\Delta w_j = w_{lj} - w_{gj}$, strongly varies with r_j. It is low in the area near the nozzle axis, which is occupied mainly by small droplets, already decelerated by the ambient air while large velocity difference remain in r_j > 30 mm where the spray is formed by large droplets. The ratio between

the gas phase Weber number and critical Weber number, calculated for droplet diameter $D_{v0.98j}$ at individual positions j, is typically 0.1 or less which means the secondary breakup in the axial distance 100 mm is completed.

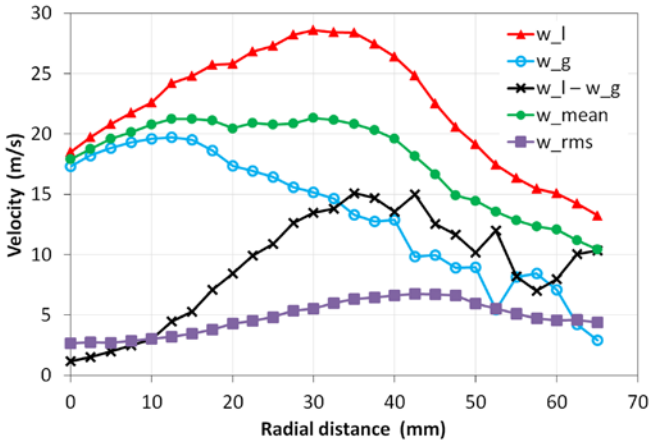

Fig. 8. Radial distributions of individual axial velocities at Δp_l = 1 MPa, spill return line closed, z = 100 mm; w_g = gas, w_l = liquid, w_{mean} = mean (for all droplets in the position), w_{rms} = root-mean-square velocity, $w_l - w_g$ = liquid to gas velocity difference.

Typical radial distribution of cumulative KE of liquid and gas phases in the spray are shown in Fig. 9. The liquid KE is concentrated in off-axis area; it reaches 50% of its total value in r_j = 41 mm while for gas it is 25 mm at Δp_l = 1 MPa. The droplets keep ~26% of the inlet energy at this regime (Table 2). This value slightly drops down with Δp_l increase as the transfer of KE from liquid into air gets more intense with increasing contact area of fine droplets and with widened SCA. The entrained air contains 10–13% of the inlet energy with the opposite trend compared to the liquid phase due to the increased energy transfer.

The total KE contained in the spray $e_{kD} + e_{kg}$ = 32–35% in agreement with [6]; it is almost independent on Δp_l., which results from relatively constant η_n and other energy values. It is by 19–25 percentage points lower than the KE at the nozzle exit, represented by η_n. This energy gap can be attributed to the dissipation within the flow and during mixing of gas with the liquid phase, partially also to turbulent, swirl and vortical air motion[7] (for its importance compare the rms with the mean velocity in Fig. 8) and entrained air flow outside the measurement boundaries. Minor part of this energy gap is attributed to the interfacial energy increase.

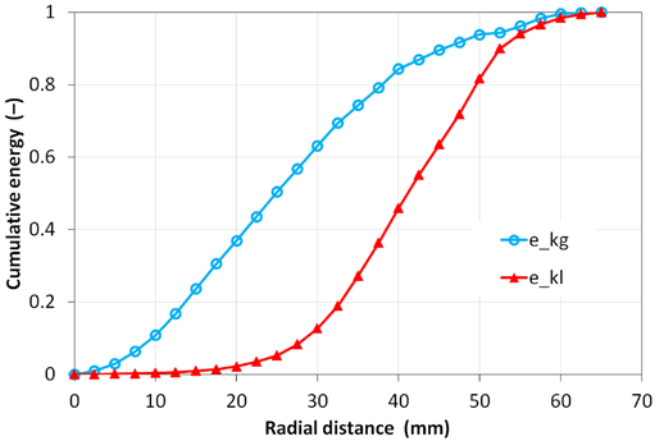

Fig. 9. Radial distributions of gas and liquid KEs in the spray (cumulative values normalised to their maximum) at Δp_l = 1 MPa, spill return line closed, z = 100 mm.

[7] These are not contained in Eq. (7).

The specific KEs of both the liquid and the entrained air markedly drop down with the opening of the spill return line as only a fraction of the pumped liquid ends in the spray (see Table 3). The reduction of the total KE with SFR increase is however much faster than the spilled out liquid quantity could simply explain. Changing the discharged fraction (1 - ε) from 0 to 31% the total KE drops to 6% of its initial value (when spill line closed). We assume that the liquid phase dispersed to the larger area (larger SCA, see Table 3) interacts more intensively with the surrounding air thus transferring there higher fraction of its original KE.

The spatial distribution of KE in the spray and variation of the KE contained in liquid and gas phases with operation conditions will have significant consequences in combustion application as it controls the fuel supply into the combustion zone as well as fuel-air interaction and the mixture preparation.

3.4. Atomization efficiency

The input energy available for the atomization process is represented by the potential energy of the supplied liquid at the pressure drop Δp_l between the atomizer inlet and exit: $E_i = V_l \Delta p_l$. This energy, as shown above, converts into the KE of liquid, partly dissipates due to viscous effects inside the atomizer and the momentum delivered to the surrounding air. Only small portion of the supplied energy ends in the surface energy of the droplets (and eventually their remaining KE) at the point of interest and can be considered as the effect of the spraying process. The amount of liquid discharged by spill-return nozzles, V_{lo}, is only a fraction of the totally supplied liquid, V_{li}, as the other part, V_{ls}, is spilled out. The energy which runs away with the spilled amount is considered lost.

The atomization process represents disintegration of bulk liquid into fine droplets, and it is associated with enormous increase of the liquid-air interfacial area[8]. The final interfacial area of a droplet system of a volume V_{lo} is $A = 6V_{lo} ID_{20}^2 / ID_{30}^3$, where ID_{20} and ID_{30} are representative surface and volume diameters respectively of the final droplets (see Eq. (A.1) in the Appendix) and the ratio ID_{30}^3 / ID_{20}^2 corresponds to the overall Sauter mean diameter, ID_{32}, as defined in Eq. (A.2) of the Appendix. The corresponding surface energy increase[9] reads $E_A = A\sigma$.

The surface energy increase divided by the inlet energy equals to the efficiency of the atomization process:

$$e_A = \eta_a = \frac{E_A}{E_i} = \frac{6V_{lo}\sigma / ID_{32}}{V_l \Delta p_l} = \frac{6\sigma(1-\varepsilon)}{\Delta p_l ID_{32}} \tag{8}$$

This formula agrees for $\varepsilon = 0$ with the equation for exergetic efficiency by [7]. It shows that the efficiency is directly related to $1/ID_{32}$, so SMD is a measure of the effectiveness of the atomization process for given liquid (determined by σ) and for given operation conditions (Δp_l, ε). The remaining KE can be eventually added to the normalised surface energy of the droplets (efficiency of the atomization process) to represent an expanded (total) effect of the atomization process in the point of interest: $\eta_a' = \eta_a + e_{kD} + e_{kg}$.

The atomization efficiency, shown in Fig. 10, left and Table 2 is less than 0.3% for the studied range of operation regimes, in accordance with [3, 6]. As suggested by the logarithmic scale of the plot, there is approximately an inverse logarithmic tendency of the η_a with the pressure drop for spill line closed, so $\eta_a \propto \exp(-\Delta p_l)$. The decrease in atomization efficiency, related with requirement of small droplets in pressure atomization, was also found by Petela [7], Rivette and Evers [4] and Michalek *et al.* [52]. The atomizer is increasingly inefficient with the spill line opening (Fig. 10, right and Table 3); the efficiency depends on the output flow rate as $\eta_a \propto \dot{Q}_{lo}^2$. It is due to the inlet energy fraction being lost in the spilled liquid; the effect of ID_{32} is weak as it remains almost constant with the spill line opening. Internally mixed twin-fluid atomizers, for comparison, based on our results [9, 53] work with $\eta_a \propto \dot{Q}_{lo}^{1.8}$ when the flow rate is controlled by GLR change at fixed Δp_l, so their efficiency decreases less markedly. Currently known PS atomizer designs, such as duplex, dual-orifice or variable-geometry [3, 35], solve this weakness but suffer from other shortcomings so a new conception to improve the flow control mechanism of PS atomizers is desired.

Based on the results in Fig. 10 the effect of pressure drop and the SFR can be empirically approximated by

$$\eta_a = 0.37(1-\varepsilon)\exp(-0.63\Delta p_l) \text{ (\%, –, MPa)} \tag{9}$$

or using the often reported correlation in Eq. (5):

$$\eta_a = 0.204(1-\varepsilon)\Delta p_l^{-0.9} \tag{10}$$

Both equations (9) and (10) fit the experimental data with an error less than 4%.

[8] For example a breakup of a liquid sphere with 10 mm in diameter into 100 micron droplets represents 100 times increase in the interfacial area.

[9] The original surface energy of bulk liquid is neglected.

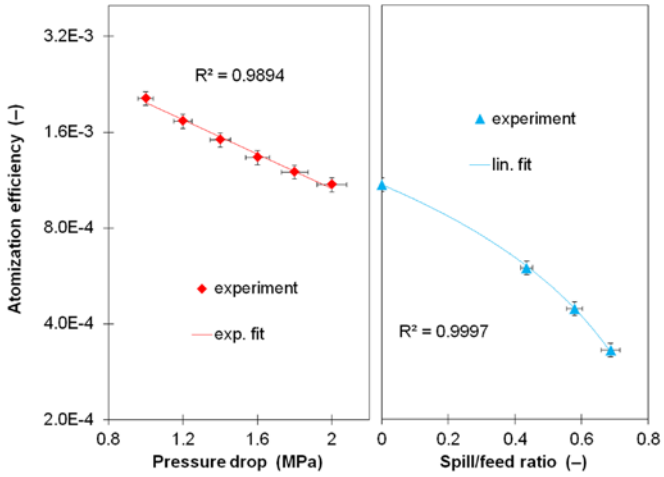

Fig. 10. Atomization efficiency at variable Δp_l with spill return line closed (left) and at variable SFR for Δp_l = 2 MPa (right). The fitting curves are provided with 4% error bars and with correlation coefficient R^2.

Results given in Fig. 10 are in good agreement with findings of others. Loefler-Mang and Leuckel [6] obtained η_a = 0.1–0.4% for spill controlled PS atomizers. Petela [7] found exergetic efficiency of pressure atomizers in the range 0.08–0.24% for pressure drops between 0.8 and 2 MPa and noted a decrease of the efficiency with the pressure drop.

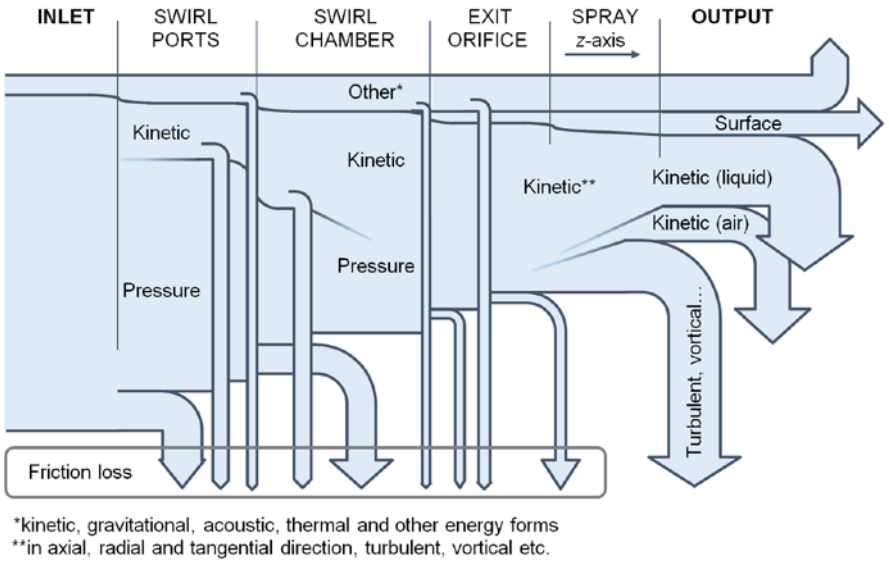

Fig. 11. Sankey diagram for energy balance of the atomization process; the energy flux proportions are illustrative, approximately corresponding to the case with SFR = 0, not to precise scale.

Two forces act against the liquid disintegration: surface tension, included in the Eq. (8), and viscosity. The effect of viscous forces depends on the atomization route. The relative importance of viscous and surface tension forces can be estimated by the ratio of the liquid phase Weber and Reynolds numbers at the nozzle exit [54]: $We_{lo}/\mathrm{Re}_{lo} = w_{lo}\mu_l/\sigma$. This ratio increases for LHO from 23 to 31.5 when Δp_l changes from 1 to 2 MPa. Its value, much larger than unity, suggests the dominance of viscous over surface tension forces during the spray formation at high velocity. It partly explains the strong negative effect of Δp_l on η_a. The requirement of small droplets, conditioned with high discharge velocity, thus naturally leads atomization efficiency to drop down. It implies a task to optimize the nozzle design for the best combination of the drop size reducing factors: high discharge velocity, thin liquid sheet and high discharge liquid turbulence. Note, for comparison with other liquids, and namely fuels frequently atomized with PS atomizers, that We_{lo}/Re_{lo} for the same atomizer operated at Δp_l = 2 MPa with water

(usable e.g. for dust emission control [55] or spray cooling [56, 57]), petrol (internal combustion engines [15, 20-22]), ethanol (used around the world commonly in fuel blends for internal combustion engines [58]), diesel fuel (regular automotive fuel [8, 16, 17]), kerosene (aviation fuel [14]) and heavy fuel oil (gas turbine engines [13], utility boilers [12], heavy engines) would be 0.6, 1.3, 2.8, 5.6, 40.4 and 1184 respectively. Liquids of lower We_{lo}/Re_{lo} would give higher η_a as the viscous resistance to the deformation and desintegration will consume smaller fraction of the inlet energy.

The energy theoretically required for atomization of a unit mass $E_A/m_l = 6\sigma/\rho_l ID_{32} = e_a \Delta p/\rho_l(1-\varepsilon)$ is in our case ~2.4 J/kg, regardless of Δp_l. The really consumed energy $E_i/m_l = \Delta p_l/\rho_l(1-\varepsilon) = E_A/e_a m_l$ is 1000 times greater than the theoretical requirement. A Sankey diagram (Fig. 11) visualizes the energy transfers between individual processes. Mutual energy transformations take place during the spray formation but are only partially depicted for the sake of clarity.

4. Conclusions

A PS atomizer was studied in simplex as well as spill-return mode with the aim to estimate individual energy ratios during the internal flow, discharge and formation of the spray. Key results were compared with available literature data and disparities, found in some cases, were explained. The most significant findings are as follows.

- The input energy in pressure atomization is given by the potential energy of the supplied liquid at a pressure drop between the atomizer inlet and exit, with neglecting effect of other energy inputs. A part of this pressure energy converts into the KE in the swirling ports with hydraulic loss in per cent scale. Significant part of the remaining pressure drop (58%) turns into the KE inside the swirl chamber. Main part of the energy loss (due to viscous effects inside the liquid and friction on the inner walls) attributes to the swirl chamber; it ends in liquid heating by several tenths of a degree Celsius and suggests a potential for improvements.
- Wide droplet size variation within the radial profile in spray was found and attributed to the droplet and gas dynamics. To characterise such wide size range with a unique parameter we introduce an integral Sauter mean diameter, ID_{32}. The ID_{32} monotonically decreases with Δp_l as $ID_{32} \propto \Delta p_l^{-0.1}$ and it is in a constant ratio to the sheet thickness at its breakup position. The radial profiles of D_{32} widen with spill line opening, but the ID_{32} remain almost constant within the studied SFR range.
- The KE of the spray at a closed spill line, 32–35% of the inlet energy, covers the droplet KE (21–26%) and KE of entrained air (10–13%); it moderately varies with Δp_l as energy transfer between droplets and air depends on the contact area of droplets. The spray KE is by 19–25 percentage points lower than the KE at the nozzle exit. This gap resides in the KE dissipation, turbulent and vortical air motion and interfacial energy increase in a small amount. The specific KEs of both the liquid and air markedly drop down with the spill line opening as only a fraction of the liquid pumped ends in the spray.
- The efficiency of the atomization process depends on the pressure drop and SFR as $\eta_a = 0.0685(1-\varepsilon)\sigma\Delta p_l^{-0.9}$ so it declines with increases in Δp_l and SFR, being less than 0.3% for the studied range of operation regimes. The drop in η_a with Δp_l suggests for quantitative change (reduction) in the energy transfer during spray formation so the disruptive forces act less effectively against the consolidating ones. We explain it with increasing effect of the viscosity compared to the surface tension when discharge velocity increases. Deeper analysis of the atomization process is required to find ways for more efficient breakup process at high pressures; optimum combination of the drop size reducing factors (high discharge velocity, thin liquid sheet and high discharge liquid turbulence) is to be found.
- The main advantages of spill-return atomizers in comparison with the simplex ones, as easy flow rate control with very large turn-down ratio and good atomization for very low flow rates, are at the expense of high energy consumption for the liquid pumping, represented with the $(1-\varepsilon)$ term, and of significant spray angle widening during the reduction from the nominal to minimal flow rate. Duplex design, swirl port switching or variable ports, control mechanism alternates of the spill function, however face other drawbacks. So after long usage of spill-return nozzles an advanced control mechanism invention is advisable.
- Several recommendations result from our findings for the nozzle design: optimum width to height ratio of swirl ports is 1/3, the minimum number of the swirl ports providing homogeneous swirling flow and uniform spray to be used, the length to width ratio of ports should be as small as possible, but minimum about 1.3. Energy loss in the swirl chamber is dominant so future investigations should focus to understand better the chamber flow and optimize the nozzle geometry to increase the nozzle efficiency (maximization of the output velocity) and reduce the sheet thickness at the nozzle exit.

PS atomizers proved to be competitive with other atomizer types in the long term due to their simple design, large turn-down ratio and good atomization characteristics. Our results show their atomization efficiency is comparable with effervescent or compound and better than that of airblast or plain orifice atomizers; however today requirements for energy processes optimization and optimal use of energy resources require innovative designs of this energy conversion device.

Acknowledgements

Authors acknowledge financial support from project No. P101/11/1264 funded by the Czech Science Foundation and NETME Centre, regional R&D centre built with the financial support from the Operational Programme "Research and Development for Innovations" within the project "NETME Centre (New Technologies for Mechanical Engineering)", Reg. No. CZ.1.05/2.1.00/01.0002 and, in the follow-up sustainability stage, supported through NETME CENTRE PLUS (LO1202) by financial means from the Ministry of Education, Youth and Sports under the "National Sustainability Programme I".

Nomenclature

A	interfacial area, cross-sectional area	(m^2)
a, b	coefficients in Eqs. (2) and (5)	(–)
b	width	(m)
c	specific heat capacity	(J/(kg·K))
c_w	velocity coefficient	(–)
D	droplet diameter	(µm)
D_{32}	Sauter mean diameter, SMD	(µm)
d	diameter	(m)
E	energy	(J)
e	energy, represented as percentages of the total input energy, specific energy	(%, –)
f_D	Darcy friction factor	(–)
h	height	(m)
ID	integral (overall) droplet diameter	(µm)
k_{p1}	width to length ratio of swirl ports	(–)
k_{p2}	length to width ratio of swirl ports	(–)
L	breakup length	(mm)
l	length	(m)
m	mass	(kg)
n	number	(–)
$\dot{Q}$	volumetric flow rate	(m^3/s, ml/s)
Re_W	Reynolds number according Walzel [34] ($=\left(2\rho_l \Delta p_l\right)^{0.5} d_o/\mu_l$)	(–)
r	radial distance from atomizer axis	(mm)
T	thermodynamic temperature	(K)
t	film thickness	(m)
V	volume	(m^3)
We	Weber number, ($We_g = \rho_g \left(w_l - w_g\right)^2 D/\sigma$)	(–)
w	velocity	(m/s)
x, y, z	Cartesian coordinates (z = axial distance)	(mm)

Greek characters

α	spray cone angle, SCA	(deg)
Δp_l	pressure differential between the atomizer inlet and exit	(MPa)
ε	spill/feed ratio, SFR, ($=V_{ls}/V_{li}$) according [6]	(–)
η_a	atomization efficiency	(%, –)
η_n	nozzle efficiency	(%, –)
μ	dynamic viscosity	(kg/(m·s))
ρ	density	(kg/m^3)
σ	liquid/gas surface tension	(kg/s^2)

Subscripts

A	surface
c	swirl chamber
D	droplet
g	gas, ambient air
i	inlet, index number
j	index of measurement position
k	kinetic (energy)
L	in the breakup distance
l	atomized liquid (light heating oil, LHO)

501 *o* exit orifice, outlet
502 *p* swirl ports
503 *s* spill-return

504 **References**

1. Jakobs, T., N. Djordjevic, S. Fleck, M. Mancini, R. Weber and T. Kolb, *Gasification of high viscous slurry R&D on atomization and numerical simulation.* Applied Energy, 2012. **93**(0): p. 449-456.
2. Lefebvre, A.H. and D.R. Ballal, *Gas turbine combustion - alternative fuels and emissions*. 2010, Taylor & Francis,: Boca Raton. p. 1 online resource (xix, 537 p.).
3. Bayvel, L. and Z. Orzechowski, *Liquid Atomization*. 1993: Taylor & Francis Inc.
4. Rivette, S.M., *Compound port fuel injector nozzle droplet sizes and spray patterns.* 1996.
5. Dumouchel, C., J. Cousin, and K.l. Triballier, *On the role of the liquid flow characteristics on low-Weber-number atomization processes.* Experiments in Fluids, 2005. **38**(5): p. 637-647.
6. Loffler-Mang, M. and W. Leuckel, *Atomization with Spill-Controled Swirl Pressure-Jet Nozzles.* ICLASS-91, Gaithersburg, MD, USA, 1991: p. 431-440.
7. Petela, R., *EXERGETIC ANALYSIS OF ATOMIZATION PROCESS OF LIQUID.* Fuel, 1984. **63**(3): p. 419-422.
8. Sovani, S.D., J.D. Crofts, P.E. Sojka, J.P. Gore and W.A. Eckerle, *Structure and steady-state spray performance of an effervescent diesel injector.* Fuel, 2005. **84**(12-13): p. 1503-1514.
9. Jedelsky, J. and M. Jicha, *Energy conversion during effervescent atomization.* Fuel, 2013. **111**: p. 836-844.
10. Lefebvre, A.H., *ENERGY CONSIDERATIONS IN TWIN-FLUID ATOMIZATION.* Journal of Engineering for Gas Turbines and Power-Transactions of the Asme, 1992. **114**(1): p. 89-96.
11. Liu, H., *Science and engineering of droplets : fundamentals and applications.* 2000, Park Ridge, N.J. Norwich, N.Y.: Noyes Publications; William Andrew Pub. xii, 527 p.
12. Ballester, J. and C. Dopazo, *Discharge coefficient and spray angle measurements for small pressure-swirl nozzles.* Atomization and sprays, 1994. **4**(3).
13. Jasuja, A.K., *ATOMIZATION OF CRUDE AND RESIDUAL FUEL OILS.* Journal of Engineering for Power-Transactions of the Asme, 1979. **101**(2): p. 250-258.
14. Rizk, N. and A. Lefebvre, *Drop-size distribution characteristics of spill-return atomizers.* Journal of Propulsion and Power, 1985. **1**(1): p. 16-22.
15. Li, T., K. Nishida, and H. Hiroyasu, *Droplet size distribution and evaporation characteristics of fuel spray by a swirl type atomizer.* Fuel, 2011. **90**(7): p. 2367 - 2376.
16. Wang, X.F. and A.H. Lefebvre, *MEAN DROP SIZES FROM PRESSURE-SWIRL NOZZLES.* Journal of Propulsion and Power, 1987. **3**(1): p. 11-18.
17. LEFEBVRE, A.H. and D. NICKOLAUS, *Fuel thermal stability effects on spray characteristics.* Journal of Propulsion and Power, 1987. **3**(6): p. 502-507.
18. Rizk, N.K. and A.H. Lefebvre, *AIRBLAST ATOMIZATION - STUDIES ON DROP-SIZE DISTRIBUTION.* Journal of Energy, 1982. **6**(5): p. 323-327.
19. Dikshit, S., S. Channiwala, D. Kulshreshtha and K. Chaudhari, *Experimental Investigations of Performance Parameters of Pressure Swirl Atomizer for Kerosene Type Fuel*. 2009. ASME.
20. Moon, S., C. Bae, E.F. Abo-Serie and J. Choi, *Internal and near-nozzle flow of a pressure-swirl atomizer under varied fuel temperature.* Atomization and Sprays, 2007. **17**(6).
21. Boyaval, S. and C. Dumouchel, *Investigation on the Drop Size Distribution of SpraysProduced by a High-Pressure Swirl Injector. Measurementsand Application of the Maximum Entropy Formalism.* Particle & Particle Systems Characterization, 2001. **18**(1): p. 33-49.
22. VanDerWege, B.A. and S. Hochgreb. *The effect of fuel volatility on sprays from high-pressure swirl injectors*. in *Symposium (International) on Combustion*. 1998. Elsevier.
23. Park, S.H., H.J. Kim, H.K. Suh and C.S. Lee, *Atomization and spray characteristics of bioethanol and bioethanol blended gasoline fuel injected through a direct injection gasoline injector.* International journal of heat and fluid flow, 2009. **30**(6): p. 1183-1192.
24. Atadashi, I.M., M.K. Aroua, A.R. Abdul Aziz and N.M.N. Sulaiman, *Refining technologies for the purification of crude biodiesel.* Applied Energy, 2011. **88**(12): p. 4239 - 4251.
25. Cooper, D., A. Yule, and J. Chinn. *Experimental measurements and computational predictions of the internal flow field in a pressure swirl atomizer*. in *Proc. ILASS-Europe*. 1999.
26. Tratnig, A. and G. Brenn, *Drop size spectra in sprays from pressure-swirl atomizers.* International Journal of Multiphase Flow, 2010. **36**(5): p. 349-363.
27. Tipler, W. and A.W. Wilson, *Combustion in Gas Turbines*, in *CIMAC*. 1959: Paris. p. 897 – 927.
28. Chen, S., A. Lefebvre, and J. Rollbuhler, *Factors influencing the circumferential liquid distribution from pressure-swirl atomizers.* Journal of engineering for gas turbines and power, 1993. **115**(3): p. 447-452.
29. Yule, A. and I. Widger, *Swirl atomizers operating at high water pressure.* International journal of mechanical sciences, 1996. **38**(8): p. 981-999.

30. Kim, S., T. Khil, D. Kim and Y. Yoon, *Effect of geometric parameters on the liquid film thickness and air core formation in a swirl injector.* Measurement Science and Technology, 2009. **20**(1): p. 015403.
31. Lee, E.J., S.Y. Oh, H.Y. Kim, S.C. James and S.S. Yoon, *Measuring air core characteristics of a pressure-swirl atomizer via a transparent acrylic nozzle at various Reynolds numbers.* Experimental thermal and fluid science, 2010. **34**(8): p. 1475-1483.
32. Dash, S., M. Halder, M. Peric and S. Som, *Formation of air core in nozzles with tangential entry.* Journal of fluids engineering, 2001. **123**(4): p. 829-835.
33. Halder, M., S. Dash, and S. Som, *Initiation of air core in a simplex nozzle and the effects of operating and geometrical parameters on its shape and size.* Experimental thermal and fluid science, 2002. **26**(8): p. 871-878.
34. Walzel, P., *Liquid atomization.* Journal Name: International Chemical Engineering (A Quarterly Journal of Translations from Russia, Eastern Europe and Asia); (United States); Journal Volume: 33:1, 1993: p. Medium: X; Size: Pages: 46-60.
35. Lefebvre, A.H., *Atomization and sprays*. Combustion,. 1989, New York: Hemisphere Pub. Corp. xi, 421 p.
36. Elkotb, M.M., N.M. Rafat, and H.M. A., *The Influence of Swirl Atomizer Geometry on the Atomization Performance.*, in *Proceedings of the first ICLASS*. 1978: Tokyo. p. 109 – 115.
37. Rizk, N. and A. Lefebvre, *Prediction of velocity coefficient and spray cone angle for simplex swirl atomizers.* International Journal of Turbo and Jet Engines, 1987. **4**(1-2): p. 65-74.
38. Horvay, M. and W. Leuckel. *LDA-measurements of liquid swirl flow in converging swirl chambers with tangential inlets.* in *2nd International Symposium on Applications of Laser Anemometry to Fluid Mechanics.* 1985.
39. Horvay, M. and W. Leuckel, *Experimental and theoretical investigation of swirl nozzles for pressure-jet atomization.* German chemical engineering, 1986. **9**(5): p. 276-283.
40. Yule, A. and J. Chinn, *The internal flow and exit conditions of pressure swirl atomizers.* Atomization and Sprays, 2000. **10**(2): p. 121-146.
41. Moon, S., E. Abo-Serie, and C. Bae, *Liquid film thickness inside the high pressure swirl injectors: Real scale measurement and evaluation of analytical equations.* Experimental Thermal and Fluid Science, 2010. **34**(2): p. 113-121.
42. Nonnenmacher, S. and M. Piesche, *Design of hollow cone pressure swirl nozzles to atomize Newtonian fluids.* Chemical Engineering Science, 2000. **55**(19): p. 4339-4348.
43. Mandal, A., M. Jog, J. Xue and A. Ibrahim, *Flow of power-law fluids in simplex atomizers.* International journal of heat and fluid flow, 2008. **29**(5): p. 1494-1503.
44. Santolaya, J., L. Aisa, E. Calvo, I. García and L. Cerecedo, *Experimental study of near-field flow structure in hollow cone pressure swirl sprays.* Journal of propulsion and power, 2007. **23**(2): p. 382-389.
45. Mandal, B., P. Barman, and A. Kushari. *Study of Primary Atomization in a Helical Passage Pressure-Swirl Atomizer*. in *19th ILASS EUROPE*. 2004.
46. Chen, S., A. Lefebvre, and J. Rollbuhler, *Factors influencing the effective spray cone angle of pressure-swirl atomizers.* ASME Transactions Journal of Engineering Gas Turbines and Power, 1992. **114**: p. 97-103.
47. Radcliffe, A., *Fuel Injection, High Speed Aerodynamics and Jet Propulsion*. 1960.
48. Babu, R.K., M.V. Narasimhan, and K. Karayanaswamy, *Prediction of Mean Drop Size of Fuel Sprays from Swirl Spray Atomizers*, in *Proceedings of the second International Conference on Liquid Atomisation and Spray Systems*. 1982: Madison, Wisconsin. p. 99-106.
49. Wang, X. and A. Lefebvre, *Influence of ambient air pressure on pressure-swirl atomization.* Atomisation Spray Technology, 1987. **3**: p. 209-226.
50. Simmons, H.C. and C.F. Harding, *SOME EFFECTS OF USING WATER AS A TEST FLUID IN FUEL NOZZLE SPRAY ANALYSIS.* Journal of Engineering for Power-Transactions of the Asme, 1981. **103**(1): p. 118-123.
51. Rizk, N. and A. Lefebvre, *Spray characteristics of spill-return atomizers.* Journal of Propulsion and Power, 1985. **1**(3): p. 200-204.
52. Michalek, D., B. Peschke, and L. Evers, *Computational design of experiments for compound fuel injector nozzles.* SAE Tech Pap, 1997. **Ser 971617**.
53. Jedelsky, J., M. Jicha, J. Slama, and J. Otahal, *Development of an Effervescent Atomizer for Industrial Burners.* Energy & Fuels, 2009. **23**: p. 6121-6130.
54. Yule, A.J. and J.J. Dunkley, *Atomization of Melts: For Powder Production and Spray Deposition*. Oxford Series on Advanced Manufacturing (Book 11). 1984, USA: Oxford University Press. 424 pages.
55. Jaber, J.O. and S.D. Probert, *Environmental-impact assessment for the proposed oil-shale integrated tri-generation plant.* Applied Energy, 1999. **62**(3): p. 169-209.
56. Abdolzadeh, M. and M. Ameri, *Improving the effectiveness of a photovoltaic water pumping system by spraying water over the front of photovoltaic cells.* Renewable Energy, 2009. **34**(1): p. 91-96.
57. Chen, Q., A. Rao, and S. Samuelsen, *H2 coproduction in IGCC with CCS via coal and biomass mixture using advanced technologies.* Applied Energy, 2014. **118**(0): p. 258-270.
58. Balat, M. and H. Balat, *Recent trends in global production and utilization of bio-ethanol fuel.* Applied Energy, 2009. **86**(11): p. 2273-2282.

505

Appendix

The SMD, the frequently used spray characteristic in mass and heat transfer studies, is reported here as a measure of atomization quality. The SMD of droplets moving through the measurement volume in a measurement position *j* is defined using general formula [1]:

$$D_{pq,j} = \sqrt[p-q]{\sum_{i=1}^{n_j} D_{ij}^{p} \Big/ \sum_{i=1}^{n_j} D_{ij}^{q}} \qquad \text{(A.1)}$$

where $p = 3$ and $q = 2$. The size spectrum of droplets generated by PS atomizer is not spatially uniform (see Figs. 6 and 7 in the main paper) so D_{32} varies along the radial profile. For the sake of conciseness and comparison of results we defined an integral value of diameters D_{32} — ID_{32}, as a single parameter to represent globally the droplet size in the spray. Note that some authors [2] use the same term while other authors refer to this overall value as the *mean* diameter [3]. Calculation of the ID_{32} is based on the surface area mean diameter and volume mean diameter $D_{20,j}$ and $D_{30,j}$ respectively, according Eq. (A.1) with corresponding p and q values, measured in axisymmetric spray, at radial positions r_j, with droplet transit frequency f_j using PDA. Simplified estimation of ID_{32} as a representation of D_{32} averaged through entire radial profile reads:

$$ID_{32} = \sum_{j=2}^{m} \left(r_j D_{30,j}^{3} f_j \right) \Big/ \sum_{j=2}^{m} \left(r_j D_{20,j}^{2} f_j \right). \qquad \text{(A.2)}$$

For the full description of ID_{32} calculation see [4] Appendix 1, which also explains simplifications and uncertainties of the method. This approach of weighting by data rate for estimation of overall D_{32} was used in [5] for estimation of the *global* SMD. Similar calculation of overall D_{32} with weighting by the cross-section area was used in [6] and [3] and previously suggested by Zaller and Klem [7] for calculation of the mean value of D_{30}.

The estimation of overall D_{32} in PS sprays depends on the method applied for the drop size measurement [8]. For example laser diffraction droplet sizing uses an expanded laser beam passing through whole the spray. This frequently used ensemble measurement technique is a concentration-based measurement. Therefore, particle velocities are not accounted for [9] and the weighting factor r_j, which covers the variation in the sprayed area with radial distance in Eq. (A.2), is not included, as well. Results acquired using such a method would, therefore, differ from these from PDA in the same spray.

References

1. Lefebvre, A.H., *Atomization and sprays*. Combustion,. 1989, New York: Hemisphere Pub. Corp. xi, 421 p.
2. Jakobs, T., N. Djordjevic, S. Fleck, M. Mancini, R. Weber and T. Kolb, *Gasification of high viscous slurry R&D on atomization and numerical simulation.* Applied Energy, 2012. **93**(0): p. 449-456.
3. Im, J.H., D. Kim, P . Han, and Y. Yoon, *Self-pulsation characteristics of a gas-liquid swirl coaxial injector.* Atomization and Sprays, 2009. **19**(1): p. 57-74.
4. Jedelsky, J., M. Jicha, J. Slama, and J. Otahal, *Development of an Effervescent Atomizer for Industrial Burners.* Energy & Fuels, 2009. **23**: p. 6121-6130.
5. Tratnig, A. and G. Brenn, *Drop size spectra in sprays from pressure-swirl atomizers.* International Journal of Multiphase Flow, 2010. **36**(5): p. 349-363.
6. Otahal, J., J. Jedelsky, J. Fiser and M. Jicha, *Efficiency of the pressure and effervescent atomization*, in *21 Annual Conference on Liquid Atomization and Spray Systems.* 2007: Mugla, Turkey. p. 76-79.
7. Zaller, M. and M. Klem, *Shear Coaxial Injector Spray Characterization, Liquid Rocket Engine Combustion Instability*, in *AIAA, Cambridge Massachusetts*. 1995. p. 191-213.
8. Fdida, N., J.B. Blaisot, A. Floch and D. Dechaume, *DROP-SIZE MEASUREMENT TECHNIQUES APPLIED TO GASOLINE SPRAYS.* Atomization and Sprays, 2010. **20**(2): p. 141-162.
9. Robart, D., S. Breuer, W. Reckers and R. Kneer, *Assessment of pulsed gasoline fuel sprays by means of qualitative and quantitative laser-based diagnostic methods.* Particle & Particle Systems Characterization, 2001. **18**(4): p. 179-189.